

Tuneable ferroelectric liquid crystal microlaser

A. V. Ryzhkova, R. Pratibha, M. Nikkhou & I. Muševič

To cite this article: A. V. Ryzhkova, R. Pratibha, M. Nikkhou & I. Muševič (2019): Tuneable ferroelectric liquid crystal microlaser, *Liquid Crystals*, DOI: [10.1080/02678292.2019.1700567](https://doi.org/10.1080/02678292.2019.1700567)

To link to this article: <https://doi.org/10.1080/02678292.2019.1700567>

 Published online: 09 Dec 2019.

 Submit your article to this journal [↗](#)

 Article views: 43

 View related articles [↗](#)

 View Crossmark data [↗](#)



Tuneable ferroelectric liquid crystal microlaser

A. V. Ryzhkova^a, R. Pratibha^b, M. Nikkhou^{b,c} and I. Muševič^{a,d}

^aCondensed Matter Department, J. Stefan Institute, Ljubljana, Slovenia; ^bSoft Condensed Matter Lab, Raman Research Institute, Bangalore, India; ^cDepartment of Physics, King's College London, London, UK; ^dFaculty of Mathematics and Physics, University of Ljubljana, Ljubljana, Slovenia

ABSTRACT

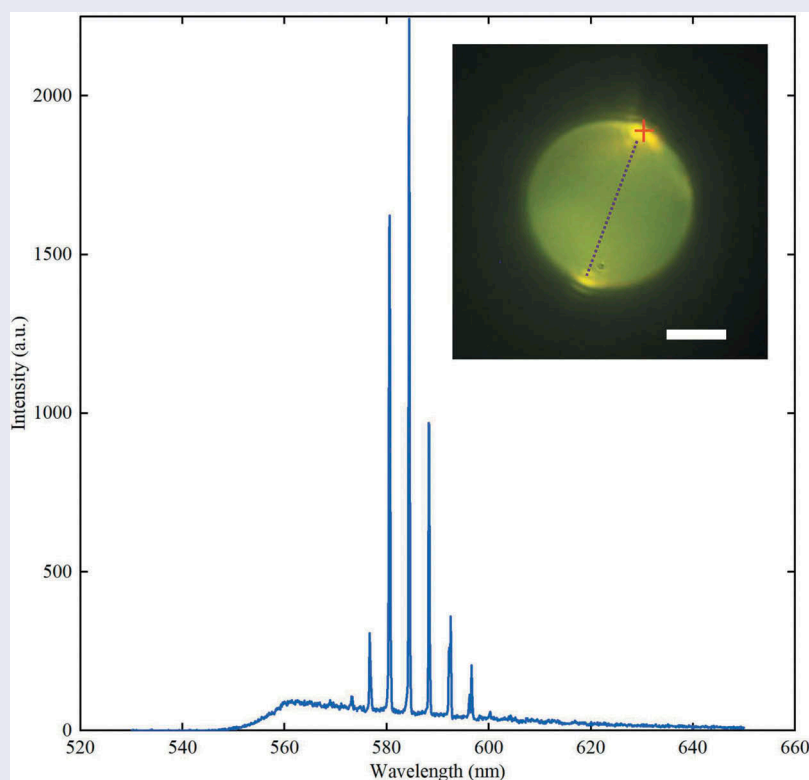
We demonstrate electric field tuning of Whispering Gallery Mode resonances in microdroplets of a dye-doped ferroelectric liquid crystal suspended in highly transparent fluorinated polymer solution CYTOP. The ferroelectric liquid crystal is a 9:1 mixture of CE3 and CE14 ferroelectric liquid crystals, exhibiting the ferroelectric Sm C* phase between 42°C and 74°C with a rather short helical pitch of 300 to 500 nm. In the Sm C* phase, the droplets show excellent optical homogeneity with perpendicular anchoring of liquid crystal molecules at the surface. Upon the excitation with a pulsed laser, the ferroelectric liquid crystal microdroplets emit laser light showing multimode WGM spectrum. When an external slowly varying electric field is applied along the direction of the excitation laser beam, we observe a red-shift of the WGM resonances, indicating an effective increase of the optical path for WGM resonant light. The shift is fully reversible, it is quadratic in the applied electric field and has a value of ~ 4.5 nm at an electric field of $2 \text{ V}(\mu\text{m})^{-1}$. It is qualitatively explained by considering the soliton-like deformation of the helical ferroelectric Sm C* structure in an external electric field.

ARTICLE HISTORY

Received 29 September 2019
Accepted 1 December 2019

KEYWORDS

Microcavities; liquid crystals; lasers; tuneable; laser sensors



1. Introduction

Lasers made of liquid crystals (LC) [1–7] are an interesting family of dye lasers, which demonstrate large

tunability of the emission wavelength, easy fabrication and flexibility in design and construction. The most studied are liquid crystal lasers made of cholesteric liquid crystals (CLCs), although lasing has been reported in

other modulated liquid crystal phases, such as Blue Phase II [8]. Cholesteric LC represents an interesting birefringent and periodic structure, which exhibits a photonic bandgap for circularly polarised light, propagating along the helical axis. When doped with an optical gain material (dye), a distributed feedback CLC laser is obtained, which emits a single wavelength along the wave-vector of helical modulation.

Another class of helically modulated liquid crystals is the ferroelectric Sm C* phase of a chiral liquid crystal (FLC), discovered by R. B. Meyer et al. in 1975 [9]. The constituent molecules must be chiral and must have an electric dipole moment in a direction perpendicular to the long molecular axis in order to form the ferroelectric liquid crystalline (FLC) phase [10,11]. In the ferroelectric phase of a liquid crystal, rod-like molecules are arranged in fluid-like smectic layers, with no positional order of molecular centres of gravity within the layers. The molecules are tilted at an angle θ with respect to the smectic normal and the spontaneous polarisation \vec{P}_s appears in a direction perpendicular to the plane of tilt, as illustrated in Figure 1(a). The chirality of LC molecules induces helicoidal precession of the local direction of LC molecules as one is moving along the normal to the smectic layers. This results in a helically modulated Sm C* structure, where on the macroscopic scale, the spontaneous electric polarisation is averaged to zero, as evident from the schematic drawing in Figure 1(b). The helical period of the Sm C* phase depends on the chirality and molecular properties, and can be in the range ~ 300 nm to several micrometres. Optically, the ferroelectric Sm C* phase is locally uniaxial material with the optical axis pointing along the long molecular axis (i.e. in a direction of local tilt). The helicoidal supramolecular arrangement averages-out the in-smectic-plane

component of the optical dielectric tensor and to a good approximation, the Sm C* phase can be considered as an effective uniaxial crystal with the birefringence that is temperature-dependent due to temperature dependence of the molecular tilt angle. In addition to birefringence, the ferroelectric Sm C* phase is a modulated phase, which gives rise to selective Bragg reflection for light propagating along the helical axis, or to Bragg diffraction for light propagating perpendicular to the helical axis. In thin layers, FLCs give rise to very fast electro-optic response, with a great potential for fast electro-optic devices [12]. FLCs have been comprehensively studied and their optics are well understood [10].

When an external electric field \vec{E} is applied along the smectic layers, it couples linearly to local spontaneous polarisation and the local free energy density changes by $-(\vec{P}_s \cdot \vec{E})$. This causes elastic deformation of the helical structure, which becomes asymmetric as shown in Figure 1(c). The regions with a preferable orientation of spontaneous polarisation grow in expense to those where the polarisation is pointing in the opposite direction. This creates the 2π soliton lattice, i.e. a linear array of regularly repeating 2π soliton walls. Within each soliton wall, the molecules rotate by the full angle 2π , as we move through that wall. The individual soliton walls are separated by nearly uniformly aligned polarisation (and tilt). Optically, the 2π soliton lattice can be considered as a uniaxial crystal, where the macroscopic optical axis is tilted with respect to the layer normal. The direction of the effective tilt of the optical axis is reversed when the direction of the external electric field \vec{E} is reversed [10].

Microlasers can be made of liquid crystals by dispersing the LC in an immiscible fluid such as water,

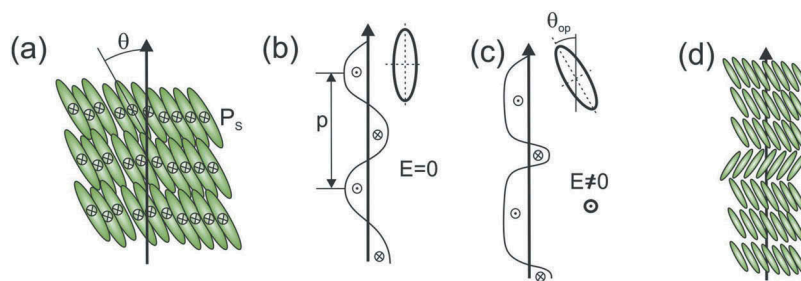


Figure 1. (Colour online) (a) Schematic drawing of a local arrangement of rod-like molecules in the Sm C* ferroelectric liquid crystal. Each molecule has an electric dipole moment that is perpendicular to the molecular structure and is on the average pointing into the plane of smectic layers. This results in collective spontaneous polarisation \vec{P}_s . (b) Due to chirality of molecules, the molecular tilt precesses, as we move along the normal to the smectic layers. This results in helical arrangement on the macroscopic scale with the helical period p in the range from ~ 300 nm to several micrometres. Effectively, the helical structure is a uniaxial crystal with the optical axis along the normal to the layers, as indicated in the upper right corner. (c) In the linear coupling regime, the helical structure is distorted and forms 2π soliton walls, when an external electric field \vec{E} is applied along the smectic layers. This is effectively a uniaxial crystal with the direction of the optical axis tilted as indicated in the upper right corner. The effective tilt angle θ_{op} is linear in $|\vec{E}|$. (d) Schematic drawing of molecular arrangement in a 2π soliton lattice.

glycerol, PDMS [13–15]. Due to surface tension, perfectly spherical droplets of LC are self-formed, which also have a perfect internal structure in terms of the LC alignment. This is due to the long-range orientational order in LC, their elasticity and well-defined orientational anchoring at the surface of the droplet. Microdroplets of nematic liquid crystal with radial director structure sustain the circulation of WGM resonances due to total internal reflection (TIR) at the interface and the resonances can be tuned by an external electric field [13].

If optical gain is added to the optical microresonator, the light will be amplified by stimulated emission during each round trip of photons and we shall obtain a WGM microlaser. Tuneable WGM microlasers are typically obtained in dye-doped radial nematic microresonators. In another case, 3D lasing has been observed from chiral and fluorescent nematic droplets, where the LC spontaneously organises into a 3D onion-Bragg microcavity [16]. Recently, magnetic field tuning of WGM resonances has been reported in droplets made of ferromagnetic nematic LC doped with fluorescent dye molecules [17].

Although lasing and tuning has been reported for a variety of bulk LC phases, including bulk ferroelectric Sm C* phase [18–20], there is only one study of lasing from microdroplets made of ferroelectric liquid crystals, recently reported by Dhara et al. [21]. In that work, a room temperature dye-doped FLC with a relatively large helical pitch of $\sim 2.8\mu\text{m}$ was used. The authors report nearly an order of magnitude lower threshold for WGM lasing, compared to the lasing threshold in dye-doped nematic microdroplets. Upon the application of an external DC electric field, the authors observed broadening of the WGM lasing lines and decrease of lasing intensity until lasing completely vanished at $\sim 0.3\text{V}/\mu\text{m}$. This was accompanied with clearly observable structural changes in the FLC droplets. No tuning and shifting of WGM resonance with the increasing electric field was reported.

In this work, we present tuning of the WGM resonances in microdroplets of a short-pitch ferroelectric liquid crystal in an external electric field. We use droplets of ferroelectric LC with the helical period in the range 300 to 500 nm, which is much shorter than the helical period used in Ref [21]. The droplets are suspended in fluorinated polymer CYTOP. The refractive index of CYTOP is 1.34 and is lower than both refractive indices of FLC, thereby sustaining the circulation of WGMs following total internal reflection of light at the FLC-CYTOP curved interface. The FLC is doped with a small concentration of a fluorescent dye that provides an optical gain for light propagating inside the ferroelectric LC microdroplet, as presented in Figure 2(c). When an external electric field is applied to the droplet, it

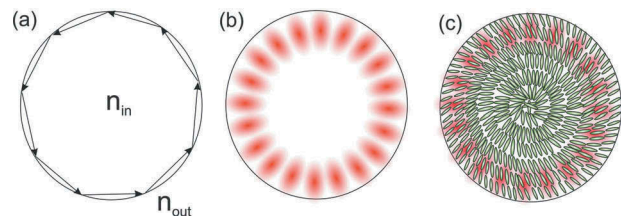


Figure 2. (Colour online) Schematic presentation of Whispering Gallery Mode resonances in spherical droplets. (a) Ray-picture of WGM resonances. Rays are reflected at the droplet interface by total reflection, because the refractive index of the droplet is higher than the outside refractive index. (b) Wave picture of WGM resonances. The WGM resonances are in this case standing-wave solutions of the wave equation in a spherical object. (c) When ferroelectric Sm C* LC forms a spherical droplet, the smectic layers are strongly curved and the helical axis is locally perpendicular to the surface of the droplet. WGMs are propagating through the near-surface layer of Sm C* material. By applying an external field, the effective refractive index of Sm C* material in the region where WGMs are circulating, changes due to soliton deformation, which in turn changes the condition for optical resonances. This results in the frequency shift of the WGM spectrum.

changes the helical structure of the ferroelectric LC material in the volume close to the surface, where the WGMs are circulating. Correspondingly, this changes the effective index of refraction for WGM propagation, which in turn changes the condition for WGM resonances. We observe WGM lasing from ferroelectric LC droplets and the spectrum is red-shifted when an external electric field is applied. The shift of WGMs does not depend on the polarity of the applied electric field and is quadratic in the electric field strength. This is in qualitative agreement with a simple model, where the FLC molecules are gradually aligned into the electric field direction, when the electric field is applied. This results in an effective tilt of the optical axis at the droplet's interface and induces an effective increase of the refractive index for WGMs, thereby red-shifting the WGM spectrum.

2. Whispering gallery modes in anisotropic microspheres

Whispering Gallery Modes in spherical droplets of isotropic material are presented in Figure 2(a). The refractive index of the droplet n_{in} must be higher than the refractive index of surrounding isotropic material n_{out} . In this case, light propagating inside the droplet can be totally reflected from the surface of the droplet. If after a series of total reflections the light returns to the origin with the same phase, the condition for an optical resonance is fulfilled. These optical eigenmodes can be considered as light circulating resonantly inside the resonant cavity and are

called Whispering Gallery Modes in accordance with spectacular acoustic resonances in domes, first observed by Lord Rayleigh [22]. The object which can sustain WGMs can be of other shapes than spherical, and the corresponding modes are also called the morphology-dependent optical modes.

In photonics, WGMs are therefore optical modes confined to very small volumes of micrometre dimensions typically and they are interesting for applications in integrated photonics [23]. Their small modal volume is characterised by large sensitivity of these resonances to any change in surface property or dimension. This sensitivity can be used for sensing applications, where the frequency shift of WGM resonances is monitored as sensor's response. WGMs have been extensively studied in nematic microdroplets, demonstrating large tuning of the spectral position of WGM resonances by an external electric field, surface adsorption of targeted molecules or change of shape of the droplet.

The theory of WGMs in optically isotropic microresonators is very well developed because of their importance in basic and applied science, see Ref. [24,25] and the references therein. In spherically symmetric and isotropic resonators, the WGMs are solutions of Maxwell's equations that appear in a form of spherical harmonic functions and spherical Bessel functions [26]. These eigen-waves are characterised by three integer mode numbers, i.e. the polar mode number (l), the azimuthal mode number (m) and the radial mode number (q). Furthermore for each mode characterised by (l, m, q) , there are two orthogonal polarisations: transverse electric (TE) and transverse magnetic (TM) polarisation. The radial mode number q counts the number of maxima of the radial intensity distribution, whereas the polar mode number l counts the number of wavelengths (oscillations in space) for one circulation.

The theory of WGMs in birefringent spherical microresonators is more complex for the general distribution of the dielectric constant tensor within the microsphere. In the case of radial distribution of the optical axis, which is realised in radial nematic droplets, the symmetry of the structure allows for the decomposition of solutions of Maxwell's equations in two sets of modes [13,27]. The TE modes are sensing the ordinary index of refraction (n_o), whereas the TM modes are sensing the extraordinary index of refraction (n_e). The spectrum of WGMs, which connects the mode numbers and the oscillation frequency of the mode is obtained from characteristic equations, which are solved numerically [13]. For radial nematic droplets, where the optical axis points into the radial direction, the characteristic equation for the TE mode is equivalent to the TE mode in an isotropic sphere with the ordinary refractive index n_o , whereas the TM mode couples to both ordinary

and extraordinary refractive indices. If the diameter $2r$ of the microsphere is large, the approximate solutions for the fundamental radial mode ($q = 1$) are given by $2\pi r n_{\text{eff}} \approx \lambda$. Here λ is the wavelength of the mode and n_{eff} is the effective refractive index for mode circulation. For each polarisation, the spectrum of WGMs appears in the form of a set of mode resonances, which are not uniformly separated. The separation of wavelengths between two consecutive modes, which is also called the Free Spectral Range (FSR) is equal to $FSR = \lambda^2 / (2\pi r n_{\text{eff}})$ [28].

Figure 2(b) is a schematic presentation of the WGM mode with radial mode number $q = 1$ and the polar mode number $l = 20$ in an optically isotropic sphere. Similarly, Figure 2(c) shows the same WGM in an Sm C* droplet with smectic layers parallel to the surface of the droplet. The electromagnetic field of $q = 1$ mode is confined close to the surface and thereby senses the near-surface dielectric tensor. One can immediately see that the wavelength of this particular WGM will depend on the local distribution of the dielectric tensor. If this changes, the conditions for the resonance condition will also change. One thereby expects that the application of an external electric field would change the director distribution, resulting in a change of the resonance condition and consequent shifting of the WGM spectrum.

3. Experimental section

3.1. Ferroelectric Sm C* material

We used a mixture of CE3 and CE14 liquid crystals (90:10 wt%), which has the phase sequence Isotropic 148.7°C Blue Phase 147.1°C Chiral nematic* 74°C Sm C* 42°C Sm X. The smectic order in the Sm C* was confirmed by X-ray scattering using the 2θ diffraction method. The helical period in the Sm C* phase is in the visible range, which is evident from Figure 3. Figure 3(a) shows optical micrographs of tens of micrometre thick layers of CE3/CE14 mixture sandwiched between two glass slides at different temperatures inside the temperature interval of the Sm C* phase. Different colours of the textures are due to selective reflection of a narrow band of light, when the sample is illuminated with white light and observed in transmission. At higher temperatures, the optical texture is coloured red and the colour changes when cooling through green and blue to deep blue at 43°C. The Sm C* phase is retained down to 42°C below which there is a phase transition into some higher ordered smectic phases.

The reflection spectra of the CE3/CE14 mixture are presented in Figure 3(b). By determining the wavelength of maximum transmission we are able to

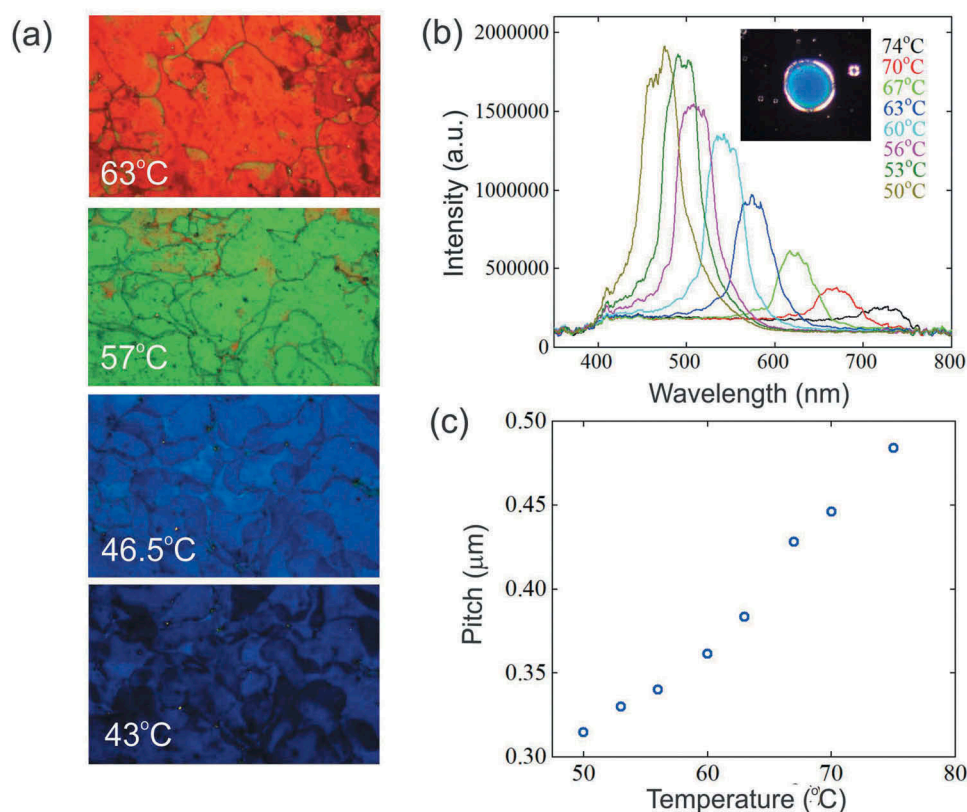


Figure 3. (Colour online) (a) Optical textures of Sm C* phase of the ferroelectric mixture (CE3/CE14,90/10) as observed in transmission and using white illumination. The colour is due to selective optical reflection, where a narrow band of circularly polarised illuminating light is reflected due to Bragg scattering from the helical birefringent structure of the Sm C* phase. Smectic layers are in this sample parallel to the slides confining the material, and the helical period of the Sm C* phase is perpendicular to the plane of the paper. (b) Reflectivity spectra measured on a tiny droplet of Sm C* mixture, attached to the surface of the glass slide. The droplet is deformed into a 'pancake'-like drop, showing uniform alignment and uniform colour (the inset). These flattened drops are attached to the surface and do not move. (c) Temperature dependence of the helical period in the Sm C* phase of CE3/CE14 mixture, as deduced from the wavelengths of maximum reflection shown in (b).

calculate the temperature dependence of the helical period in the Sm C* phase, as presented in Figure 3(c). The helical period of the Sm C* phase is in the visible range and is shifting to the blue upon cooling.

3.2. Preparation of ferroelectric Sm C* droplets for WGM lasing experiments

The main challenge of the experiment is to prepare stable droplets of Sm C* material, which are doped with a small amount of a laser dye and which are stable for a long period of time in a carrier medium. Furthermore, one has to assure that the layered structure of the Sm C* phase is neatly packed into a spherical volume of the droplet in an onion-like manner. This is only possible if the layers are parallel to the surface of the droplet and form a sequence of concentric shells of layers, packed into an onion-like fashion. Taking into account that the LC molecules are tilted at some angle θ with respect to the layer normal, the

surface anchoring of LC molecules at the interface has to be flexible to allow for temperature variations of the molecular tilt with respect to the surface normal. Temporal stability of WGM resonance in nematic droplets, suspended in various liquids has been studied by Dhara et al. [29]. It was convincingly demonstrated that fluorinated fluids, such as CYTOP, do not mix with cyanobiphenyl nematic liquid crystals, and give very stable radial nematic droplets.

We have also tested various carrier fluids for their chemical compatibility with this particular ferroelectric mixture, including glycerol and CYTOP. When droplets of ferroelectric mixture are dispersed in glycerol, one has to add around 0.75% of CTAB to assure good anchoring of smectic layers parallel to the surface of the droplet. Although we could obtain good optical quality of ferroelectric liquid crystal droplets in glycerol with CTAB, the application of a slowly varying electric field caused the electric breakdown of cells filled with

glycerol. For this reason, we chose CYTOP, which is an excellent electrically insulating fluid and could withstand large electric fields used in our experiments.

We used CYTOP CTX-809A polymer solution with $\sim 9\%$ of added fluorinated solvent in all lasing experiments reported in this article. CYTOP is an amorphous fluoropolymer with excellent electric and optical properties and it is supplied as a viscous solution of fluorinated polymer in a solvent. The solution is not very volatile and we had no problems related to solvent evaporation in our experiments that lasted typically 1 day. Because CYTOP is a completely fluorinated polymer, one expects excellent immiscibility with hydrogenated materials, such as CE-N ferroelectric liquid crystals. Immiscibility of fluids is very important when droplets of one fluid are dispersed in another fluid because of possible diffusion of material across the interface and consequent change of the diameter of droplets. CYTOP shows excellent transparency in the near IR, visible and UV region up to 200 nm. The refractive index in the visible is 1.34, which makes it an ideal material for studying WGM resonances in liquid crystalline droplets. The two refractive indices of typical CE-N liquid crystals are higher than 1.5 [30], which makes a reasonably high refractive index difference of ~ 0.2 between the ferroelectric liquid crystal droplet and the surrounding fluid.

First, a small quantity of fluorescent dye was added to the ferroelectric mixture. Several lasing dyes were tested for their miscibility with LC and immiscibility with the carrier fluid. In the experiment, the dye should not diffuse out of the ferroelectric LC droplets and into the surrounding fluid. Nile Red shows good solubility in CE ferroelectric mixture and low solubility in glycerol. Rhodamine 6G shows good solubility in CE liquid crystals, but we noticed that it also diffuses out of droplets into glycerol. Finally, Pyrromethene 580 laser dye was selected for best chemical compatibility with CE liquid crystals and low diffusion/solubility in CYTOP.

A solution of $\sim 0.1\%$ of Pyrromethane 580 dye in ethanol was added to the CE3/CE14 mixture and mixed while heated to 60°C for several hours. This helped the solvent to evaporate and leave behind well-dissolved dye in the ferroelectric LC.

The dispersion of ferroelectric droplets in CYTOP was prepared by quickly heating the crumbled FLC to 100°C on a glass slide. After liquifying, the FLC was transferred to heated CYTOP, manually stirred with a needle and cooled down to 85°C . If this was done at lower temperatures, the structural properties of droplets were poor. In this way, one can obtain a good dispersion of ferroelectric LC droplets suspended in CYTOP, as presented in Figure 4(a,b). The dispersion was then introduced between two flat glass slides with transparent ITO electrodes on their inner surfaces. The gap between the slides was $\sim 50\mu\text{m}$. A glass cell filled with CYTOP dispersion of ferroelectric LC droplets was placed on a glass slide with a transparent layer of ITO serving as a heater. The temperature of the ITO was measured by a Pt-100 resistor and was controlled by an Oxford Instruments ITC 503 temperature controller. The sample with ITO heater was placed on an inverted Nikon inverted polarising microscope with Plan Fluor ELWD 60x/0.70 objective.

3.3. Optical set-up

A schematic diagram of the optical set-up is shown in Figure 5. The set-up is based on an inverted microscope (Nikon Eclipse TE2000-U). A single ferroelectric Sm C* microdroplet was observed under an optical microscope (Figure 4(a,b)) and illuminated by a pulsed laser. The pumping laser was slightly focused through a $60\times$ air objective to an area of $\sim 20\mu\text{mm}$ diameter, thus illuminating the edge of a selected droplet. An actively Q-switched doubled Nd:YAG laser with a pulse length of 1 ns, a repetition rate of 50 Hz and a maximum pulse energy of $10\mu\text{J}$ were used as the excitation source

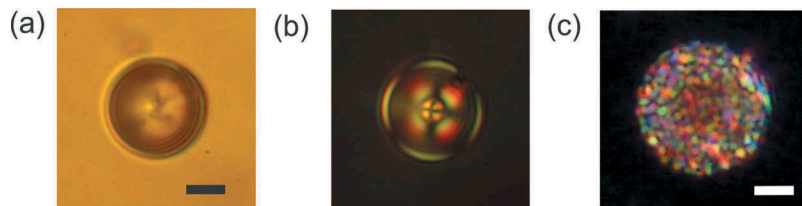


Figure 4. (Colour online) Microdroplet of a mixture of CE3 and CE14 liquid crystals (90:10 wt%) in the ferroelectric Sm C* phase at $T = 53^\circ\text{C}$, dispersed in CYTOP CTX-809A polymer solution: (a) The droplet is viewed in unpolarised light. No surfactants were added to CYTOP and the droplet is free of any visual defects. (b) The same droplet between crossed polarisers shows an excellent alignment of the ferroelectric Sm C* phase in spite of curved geometry of the droplet with finite Gaussian curvature. (c) If the droplet is in the chiral nematic phase at higher temperature $T = 75^\circ\text{C}$, it shows many defects because of the incompatibility of homeotropic surface anchoring and the chiral nematic phase, confined to a sphere. Scale bars $5\mu\text{m}$.

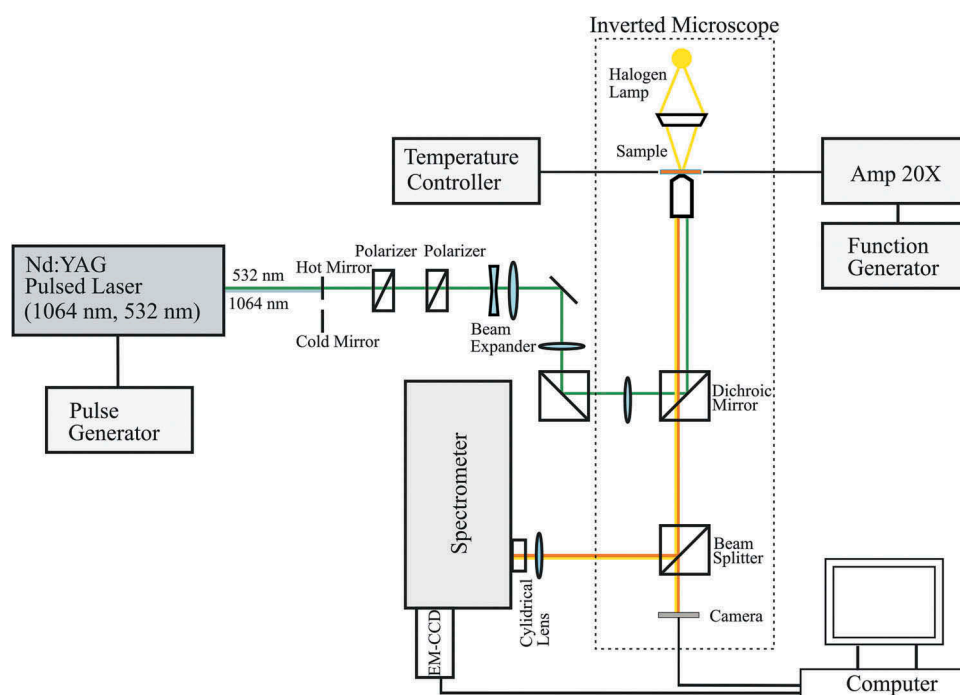


Figure 5. (Colour online) Schematic diagram of the experimental set-up for tuning the lasing wavelength from a single ferroelectric droplet by applying an external electric field.

(Alphas, Pulselas-A-1064-500). The laser was triggered by an external pulse generator and the pulse energy was determined by a pair of polarisers, which were acting as a variable attenuator. The spectra of the light, emitted by the droplet, were measured using an imaging spectrometer with a 0.05 nm resolution (Andor, Shamrock SR-500i) and cooled EM-CCD camera (Andor, Newton DU970N). The spectra were collected every 1 s from the whole volume of the droplet. The images were taken with Cannon EOS 550D equipped with 2.3 magnification lens that was mounted in front of Cannon camera.

The ITO electrodes of the cell containing the CYTOP dispersion of ferroelectric Sm C* droplets were connected to the voltage source providing different waveforms. A triangular and bipolar voltage was used in the experiments with a period of 20 s. The voltage was applied using arbitrary waveform generator DG1022, Rigol and the signal was amplified by a voltage amplifier (F10A, FLC Electronics). At the start of each experiment, the voltage generator and the Andor acquisition software were initiated at the same time. From the continuously recorded spectra, we were able to reconstruct the electric-field dependence of the collected spectra.

3.4. Results and discussion

One can see from polarised image of a ferroelectric droplet in Figure 4(b) that the director structure is radial, with a +1 radial hedgehog defect in the centre of the droplet. This

implies homeotropic anchoring of LC molecules at the interface between the CYTOP and the CE mixture. More precisely, the smectic layers are parallel to the curved surface of the droplet and because of the molecular tilt in the ferroelectric Sm C* phase, the LC molecules are tilted with respect to the local normal to the droplet's surface. This means that the homeotropic anchoring at CYTOP is flexible enough to allow for local tilting of the molecules away from the surface normal.

Interestingly, the curvature of the spherical confinement is compatible with smectic layer deformation, because the optical quality of droplets in the Sm C* phase is excellent and there are no signs of defects related to smectic order. Because the smectic layers follow the curved surface of the droplet, there is a Gaussian curvature of smectic layers $K = 1/R^2$. This curvature is positive for each smectic layer, and the inner-most smectic layers are exhibiting divergent Gaussian curvature $K \rightarrow \infty$, because the radius of inner layers vanishes, $R \rightarrow 0$.

When a selected ferroelectric Sm C* droplet is illuminated and excited with 532 nm pulsed light, one can observe characteristic and bright fluorescence and the two very bright spots, as seen from the inset to Figure 6. The brighter (upper) spot is the place where the rim of the droplet is illuminated by the focused 532 nm light (red cross). One can clearly see another bright fluorescent spot on the opposite side of the droplet. This is a clear sign of Whispering Gallery Modes, circulating inside the droplet and being totally reflected from the LC-CYTOP

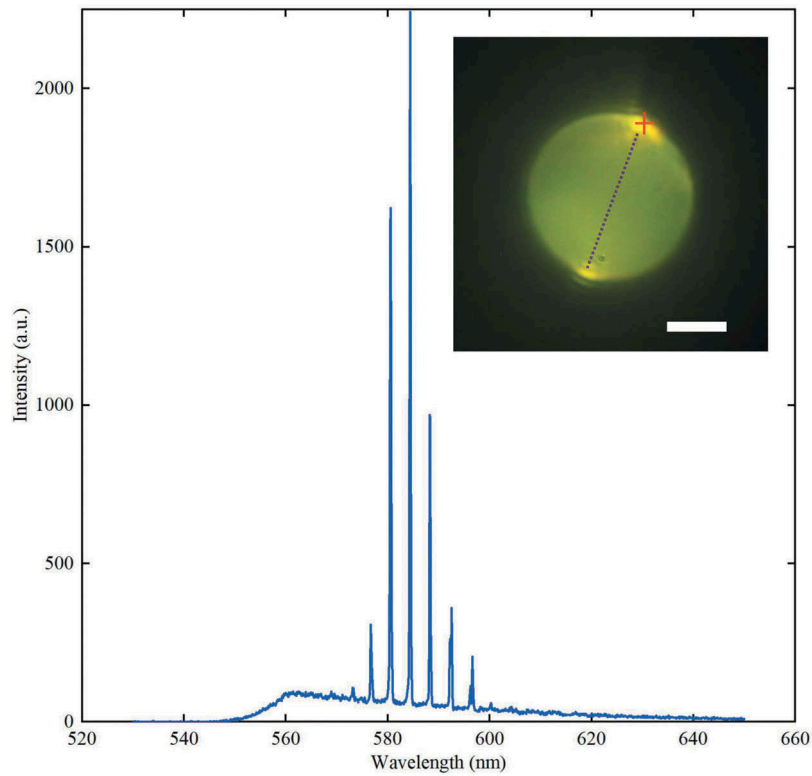


Figure 6. (Colour online) Spectrum of WGM lasing from a droplet in the ferroelectric Sm C* phase. The inset shows nonpolarized photograph of the droplet showing strong fluorescence and the two bright spots, which are the cross-sections of the WGM ring. The red cross indicates the position where the droplet was illuminated with a 532 nm beam. The purple broken line indicates the plane of WGM circulation. Scale bar 5 μm .

interface. The two bright spots are actually the cross-sections of WGM ring of light circulating inside the droplet. The refractive indices of thermotropic LCs are significantly higher than the refractive index of CYTOP, which provides good refractive index difference and strong confinement of WGMs by TIR.

The light emitted from the bright spots was collected by the microscope and the spectrum is shown in Figure 6. It clearly shows a series of narrow lines, characteristic of the WGM spectrum of the droplet. Furthermore, the intensity of the lines and the presence of speckles on captured images clearly demonstrate that we are in the lasing regime of WGMs, as previously reported in a number of publications [16,17,21].

When an external slowly varying electric field is applied to the droplets, the WGM spectrum shifts into the red, as shown in Figure 7. Here, the spectrum was recorded continuously while the applied electric field was ramped linearly and periodically from zero to the maximum value and then back to zero and towards negative values. The time period was 20 s. The electric field dependence of WGM frequencies is clearly quadratic and does not depend on the direction of the field, i.e. voltage polarity. The maximum measured shift is ~ 4.5 nm at

an applied electric field strength of ~ 2 (V/ μm). This red-shift of WGM resonances in ferroelectric Sm C* droplets is of somewhat lower magnitude but opposite to the blue-shift of WGM resonances, observed by Humar et al. [13] in radial nematic droplets.

We have not observed any structural changes in this short-pitch ferroelectric LC material, the droplets did not visually change during the application of the field. The only experimental problem was drifting of microdroplets out of focus, which is due to the electrophoretic force on a sphere suspended in a fluid. For this reason, the intensity of WGM lines could be corrected by readjusting the focus.

The observed red-shift of WGM resonances with increasing electric field indicates that the optical path for a given WGM is increasing with increasing electric field, which implies an increase of the effective refractive index for that particular WGM. This can be understood by considering a simple ray optics picture where the total optical path of a ray bouncing by TIR from the surface of the microsphere equals to $2\pi R n_{\text{eff}}$ [29]. Here R is the radius of the microdroplet and n_{eff} is the effective refractive index for WGM circulation. For a given WGM with frequency ν and wavelength λ , this optical path should equal to a $l \cdot \lambda$, where l is an

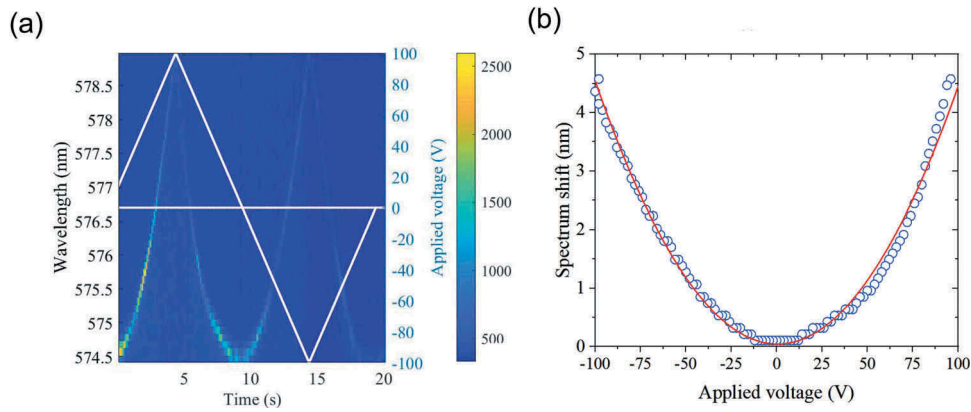


Figure 7. (Colour online) (a) Time (and also voltage/field) dependence of the spectrum of WGM lasing from a $9\ \mu\text{m}$ diameter microdroplet of the ferroelectric Sm C^* taken at 52°C . The electrical field increases and decreases in a triangular fashion, with the amplitude of $100\text{V}/50\ \mu\text{m}$, as shown in the same graph. The spectrum shifts quadratically and towards the red, i.e. longer wavelengths. (b) The magnitude of the WGM shift as a function of the applied voltage for a $9\ \mu\text{m}$ diameter ferroelectric Sm C^* droplet. This voltage was applied across $50\ \mu\text{m}$ cell, which means that the maximum value of the electric field was $2\ \text{V}/\mu\text{m}$. The solid line is a parabolic fit to the data.

integer, called the mode number. Any increase of n_{eff} thereby causes red-shift of the WGM spectrum to longer resonant wavelengths λ .

This increase of the refractive index can be explained by the linear coupling of the external slowly varying electric field with the local spontaneous electric polarisation of the Sm C^* phase and the formation of 2π soliton lattice. Briefly, the WGMs are circulating in a plane that is parallel to the direction of the applied electric field, as shown in the inset to Figure 6. The external slowly varying electric field will induce an out-of-plane of circulation tilting of molecules, which will be more and more effective as the electric field is increased. This means that the effective dielectric constant for Transverse Electric (TE) WGMs will increase with an increasing electric field, thereby red-shifting the WGM spectrum. Precise calculation of the red-shift is quite difficult, because the WGMs are circulating in a plane that is parallel to the direction of the applied electric field. It implies analytic solutions of the sine-Gordon equation for the phase profile $\phi(z)$ describing winding of the helical structure along the helical axis. At zero field the solutions are simple plane waves $\phi(z) = k \cdot z$; however, by increasing the electric field, the solutions become Jacobi elliptic functions, as described on page 117 in Ref [10]. Another complication is that the coupling between the field \vec{E} and the spontaneous polarisation \vec{P}_s will be different for different points on the trajectory of WGMs. A total change of the optical path for WGMs circulating in an external electric field is obtained by integrating the optical path along the WGM trajectory and is beyond the scope of this work.

We should also comment that we have performed the same type of experiments on microdroplets of

a long pitch ferroelectric liquid crystal SCE7. This is a room temperature FLC which has a relatively large pitch, of the order $2\text{--}3\ \mu\text{m}$. The droplets of SCE 7 were dispersed in CYTOP and the onion-like structure of the Sm C^* phase was clearly observed, due to large helical period. This onion-like structure confirms that smectic layers are parallel to the surface of the droplet and the helical modulation is in the radial direction. When the electric field was applied to these long pitch ferroelectric droplets, the WGM spectrum did not show repeatable behaviour in different experiments. The shift of the WGM spectrum with the applied electric field was quite erratic and we could estimate the maximum shift of $\sim 2.5\ \text{nm}$ at an applied field of $1.7\ \text{V}(\mu\text{m})^{-1}$. This is $\sim 30\%$ smaller response of SCE7 compared to the CE3/CE14 mixture. Moreover, SCE7 droplets showed in some cases blue shift of the WGM spectrum and in other cases, the red-shift was observed. This indicates that the optics and the mechanism of helical unwinding are quite complex in droplets with large pitch FLC compared to very short-pitch FLC materials. One of the possible reasons is good spatial homogeneity of optical properties in short-pitch FLC due to efficient spatial averaging of helical modulation.

4. Conclusion

In conclusion, we have succeeded in preparing good optical quality ferroelectric Sm C^* liquid crystal droplets and demonstrated WGM lasing. The optical resonances can be continuously and reversibly tuned by the application of an external slowly varying electric field. The red-

shift of the WGM spectrum under applied electric field is consistent with linear coupling between the external electric field and spontaneous polarisation of the Sm C* phase. This coupling distorts the smooth helical structure of the Sm C* phase into a 2π soliton lattice. The magnitude of the shift is similar to that observed in radial nematic LC microresonators for similar strengths of the applied electric field. The reversible tuning of WGM spectrum in ferroelectric LC droplets could be interesting for application in fast modulated microlasers and filters, because ferroelectric Sm C* liquid crystals are well known for their fast electro-optical response. This work is, therefore, another step towards the realisation of soft matter microphotonic elements and their integration in soft matter photonic devices.

Disclosure statement

No potential conflict of interest was reported by the authors.

Funding

This work was partially funded by Slovenian Research Agency (ARRS) (P1-0099, L1-8135).

ORCID

M. Nikkhou  <http://orcid.org/0000-0003-4475-3154>

References

- [1] Kopp VI, Fan B, Vithana HKM, et al. Low-threshold lasing at the edge of a photonic stop band in cholesteric liquid crystals. *Opt Lett*. 1998;23:1707–1709.
- [2] Taheri B, Munoz AF, Palffy-Muhoray P, et al. Low threshold lasing in cholesteric liquid crystals. *Mol Cryst Liq Cryst Sci Technol*. 2001;358:73–82.
- [3] Alvarez E, He M, Munoz AF, et al. Mirrorless lasing and energy transfer in cholesteric liquid crystals doped with laser dyes. *Mol Cryst Liq Cryst Sci Technol*. 2001;369:75–82.
- [4] Morris SM, Ford AD, Pivnenko MN, et al. Enhanced emission from liquid-crystal lasers. *J Appl Phys*. 2005;97:023103.
- [5] Jeong SM, Ha NY, Takanishi Y, et al. Defect mode lasing from a double-layered dye-doped polymeric cholesteric liquid crystal films with a thin rubbed defect layer. *Appl Phys Lett*. 2007;90:261108.
- [6] Araoka F, Shin K-C, Takanishi Y, et al. How doping a cholesteric liquid crystal with polymeric dye improves an order parameter and makes possible low threshold lasing. *J Appl Phys*. 2003;94:279–283.
- [7] Coles H, Morris S. Liquid-crystal lasers. *Nat Photonics*. 2010;4:676.
- [8] Cao W, Munoz A, Palffy-Muhoray P, et al. Lasing in a three-dimensional photonic crystal of the liquid crystal-line blue phase II. *Nat Mater*. 2002;1:111–113.
- [9] Meyer RB, Liebert L, Strzelecki L, et al. Ferroelectric liquid crystals. *J De Physique Lett*. 1975;36:69–71.
- [10] Muševič I, Blinc R, Zeks B. The physics of ferroelectric and antiferroelectric liquid crystals. Singapore: World Scientific; 2000.
- [11] de Gennes PG, Prost J. The physics of liquid crystals. Oxford: Oxford University; 1993.
- [12] Clark NA, Lagerwall ST. Submicrosecond bistable electrooptic switching in liquid crystals. *Appl Phys Lett*. 1980;36:899–901.
- [13] Humar M, Ravnik M, Pajk S, et al. Electrically tunable liquid crystal optical microresonators. *Nat Photonics*. 2009;3:595.
- [14] Humar M, Muševič I. Surfactant sensing based on whispering-gallery-mode lasing in liquid-crystal microdroplets. *Opt Express*. 2011;19:19836–19844.
- [15] Muševič I. Integrated and topological liquid crystal photonics. *Liq Cryst*. 2014;41:418–429.
- [16] Humar M, Muševič I. 3D microlasers from self-assembled cholesteric liquid-crystal microdroplets. *Opt Express*. 2010;18:26995–27003.
- [17] Mur M, Sifi JA, Kvasic I, et al. Magnetic-field tuning of whispering gallery mode lasing from ferromagnetic nematic liquid crystal microdroplets. *Opt Express*. 2017;25:1073–1083.
- [18] Kasano M, Ozaki M, Yoshino K, et al. Electrically tunable waveguide laser based on ferroelectric liquid crystals. *Appl Phys Lett*. 2003;25:4026–4028.
- [19] Ozaki M, Kasano M, Ganzke D, et al. Mirrorless lasing in a dye-doped ferroelectric liquid crystal. *Adv Mater*. 2002;14:306–309.
- [20] Ford AD, Morris SM, Pivnenko MN, et al. A comparison of photonic band edge lasing in the chiral nematic N* and smectic C* phases. *Proc SPIE*. 2004;5289:213–220.
- [21] Sofi JA, Dhara S. Stability of liquid crystal micro-droplets based optical microresonators. *Appl Phys Lett*. 2019;114:091106.
- [22] Lord R. The problem of the whispering gallery. *Phil Mag*. 1910;20:1001–1004.
- [23] Vahala K. Optical microcavities. *Nature*. 2003;424:839–846.
- [24] Heebner J, Grover R, Ibrahim T. Optical microresonators: Theory, Fabrication and Applications. London: Springer; 2008.
- [25] Schunk G, Fürst JU, Förtsch M, et al. Identifying modes of large whispering-gallery mode resonators from the spectrum and emission pattern. *Opt Express*. 2014;22:30795–30806.
- [26] Oraevsky AN. Whispering-gallery waves. *Quant Electron*. 2002;32:377–400.
- [27] Cohoon DK. An exact solution of Mie type for scattering by a multilayer anisotropic sphere. *J Electromagnet Wave*. 1989;3:421–448.
- [28] Sofi JA, Mohiddon MA, Dutta N, et al. Electrical and thermal tuning of quality factor and free spectral range of optical resonance of nematic liquid crystal microdroplets. *Phys Rev E*. 2017;96:022702.
- [29] Sofi JA, Dhara S. Electrically tunable liquid crystal optical microresonators. *Liq Cryst*. 2019;46:629–639.
- [30] Chilaya G. Experimental investigations of some optical properties in liquid crystals with spiral structure. *Il Nuovo Cimento*. 1988;10D:1263–1271.